Australian New Year's PyroCb Impact on Stratospheric Composition

Australian New Year's PyroCb Impact on Stratospheric Composition

Michael J. Schwartz[1], Michelle L. Santee[1], Hugh C. Pumphrey[2], Gloria L. Manney[3,4], Alyn Lambert[1], Nathaniel J. Livesey[1], Luis Millán[1], Jessica L. Neu[1], William G. Read[1], Frank Werner[1]

[1]Jet Propulsion Laboratory, California Institute of Technology, 4800 Oak Grove Drive, Pasadena, CA 91109, USA
[2]School of GeoSciences, The University of Edinburgh, Edinburgh, UK
[3]NorthWest Research Associates, Socorro, New Mexico
[4]Department of Physics, New Mexico Institute of Mining and Technology, Socorro, New Mexico

Key Points:

- MLS observed record-high stratospheric trace gas abundances from the 2019-2020 Australian New Year's fires rising to 5.6 hPa over 110 days
- Plume fragments moved poleward but do not appear to have entered the developing Antarctic winter vortex
- Analysis of correlations between constituent measurements requires consideration of their spatial resolutions

Corresponding author: Michael J. Schwartz, michael.j.schwartz@jpl.nasa.gov

This article has been accepted for publication and undergone full peer review but has not been through the copyediting, typesetting, pagination and proofreading process which may lead to differences between this version and the Version of Record. Please cite this article as doi: 10.1029/2020GL090831

Abstract

Following the Australian New Year's pyrocumulonimbus complex between 29-Dec-2019 and 4-Jan-2020, the Aura Microwave Limb Sounder (MLS) observed a plume with unprecedented enhancements of H_2O and biomass-burning products (CO, HCN, CH_3Cl, CH_3CN, and CH_3OH) in the lower/middle stratosphere, accompanied by depressions in stratospheric species (O_3 and HNO_3). The plume persisted for ∼110 days, circling the globe twice while ascending to 5.62 hPa (∼35 km). Air masses drawn off the main plume moved toward the developing Antarctic polar vortex but do not appear to have penetrated it. Comparison of species in the plume requires consideration of their measurements' spatial resolutions and background abundances. The apparent decay of some long-lived plume constituents is largely attributable to their coarsening spatial resolution with height, which reduces observed peak values. Differing HCN/H_2O signatures indicate that multiple early plumes originated from different stratospheric injection events.

Plain Language Summary

Severe wildfires can trigger vigorous smoke-infused thunderstorms called pyrocumulonimbuses (pyroCbs) that rapidly loft polluted air from the surface, in the most extreme cases depositing it in the lower stratosphere ($\gtrsim$14 km altitude). Three times in the past 16 years, long-lived stratospheric plumes from major pyroCbs have been observed in a suite of biomass-burning products measured by the Microwave Limb Sounder on NASA's Aura satellite. Dark smoke in these plumes absorbs sunlight; the plumes rise because they are warmer than the surrounding air. The third, and by far the largest, of these plumes was produced by an extraordinary set of pyroCbs in Australia between 29-Dec-2019 and 4-Jan-2020, collectively known as the Australian New Year's event (ANY). The ANY plume core remained remarkably compact, circling the globe twice while rising from ∼14 km to ∼35 km altitude over a period of four months. Record-setting concentrations of five biomass-burning products were measured by MLS throughout the lower stratosphere. Plume fragments tended to move south, but do not seem to have influenced ozone-hole chemistry. Differing gas mixtures suggest that several plumes in the first month originated in different pyroCbs. Careful comparison of plume gases requires consideration of the blurriness of the measurements.

1 Introduction

Three times in the past 16 years, parcels of smoke and other fire emissions injected above the tropopause by extreme pyrocumulonimbus (pyroCb) events (Fromm et al., 2010) were persistent and absorptive enough that heating by solar radiation lofted them further into the stratosphere (Yu et al., 2019). Resulting long-lived perturbations of stratospheric composition were observable by satellite-based atmospheric sensors, including the Aura Microwave Limb Sounder (MLS). The 2009 Australian "Black Saturday" pyroCb event (BS) (Pumphrey et al., 2011), the 2017 Pacific Northwest Event (PNE) (Peterson et al., 2018; Pumphrey et al., 2020), and the 2019–2020 Australian New Years pyroCb complex (ANY) (Kablick et al., 2020, hereinafter K20) successively rewrote the record books for stratospheric perturbations of biomass burning products and plume ascent rate in the 16-year MLS data set. The ANY event was an outbreak of at least 18 pyroCbs (K20) at the peak of Australia's historic 2019–2020 "Black Summer" fire season between 29-Dec-2019 and 4-Jan-2020 that produced a stratospheric plume with MLS mixing ratios of CO, H_2O, HCN, CH_3CN, CH_3Cl, and CH_3OH that far exceeded records set by the PNE in the lower-middle stratosphere. The plume was also observable in other tropospheric tracers (N_2O) and deficits of stratospheric tracers (O_3, HNO_3). The densest part of the plume (P1, after K20) remained a sharply defined, localized, coherent feature in the composition perturbations, reaching 6.81 hPa within 70 days and observable in MLS H_2O and HCN measurements for at least 110 days. As shown by K20 and Allen

et al. (2020), solar heating of absorptive aerosol not only caused the plume to rise into the middle stratosphere, but also produced an encircling anticyclonic eddy ∼1000 km across that served as a transport barrier, contributing to the months-long persistent coherence of the trace-gas anomalies. In this work, we use MLS data to examine composition anomalies associated with the three major pyroCb events, focusing on ANY.

2 Data

Since its launch in 2004, MLS (Waters et al., 2006) has provided profiles of 15 atmospheric gas-phase constituents, cloud ice, and temperature with nearly continuous daily, near-global coverage. We use MLS v4.2 products, screened as recommended by Livesey et al. (2020), with additional screening of 11 anomalous profiles associated with instrument operations (see Supporting Information, hereinafter "SI", Table S1). Plume enhancements can be orders of magnitude larger than typical variability, assuaging concerns related to lack of sensitivity and/or biases, thus allowing scientific use of products at pressure levels that are not usually recommended (e.g., HCN at 100–31.6 hPa and CH_3CN at 100–68.1 hPa). Winds and potential vorticity (PV) are from the Modern Era Retrospective-analysis for Research and Applications, Version-2 (MERRA-2) (Gelaro et al., 2017).

3 Results

3.1 Outliers of CO and H_2O

Figure 1 shows that the three pyroCb events stand out in the MLS lower stratospheric record of CO and H_2O. Panels 1a and 1n are time series of monthly global histograms of 46.4 hPa CO and H_2O, respectively. Stratospheric CO mixing ratios in the BS plume were unprecedented in the first 13 years of the MLS record, exceeding 200 ppbv at 46.4 hPa. The 2017 PNE plume had similar maxima but was observable in MLS data for a much longer period and is estimated to have injected twice as much CO above 215 hPa as did BS (Pumphrey et al., 2020). Using the same approach, we estimate that the total CO injected by ANY is another ∼4× larger than that by the PNE, both above 215 hPa and above 100 hPa, with observed maxima at 46.4 hPa reaching 700 ppbv, against typical background abundances of ∼20±10 ppbv.

Outside of the intervals impacted by these three events, the largest enhancements in the MLS 46.4 hPa CO record are associated with descent of high CO from the mesosphere into the winter polar vortices, with significant interannual variability in the strength and persistence of this descent. Indeed, enhancements exceeding 100 ppbv in Apr–May (Figure 1a) are not related to the Jan–Feb ANY plume, but rather arise from descent of high CO air to 46.4 hPa in the unusually long-lived 2019–2020 Arctic vortex (Lawrence et al., 2020; Manney et al., 2020).

Figures 1b–m show daily histograms covering the first 110 days after the three injection events on four MLS CO retrieval levels in the lower-middle stratosphere; we focus on the pyroCb plumes, so winter latitudes (20°N–90°N for BS and ANY and 90°S–20°S for PNE) are excluded. Panels 1j–m highlight the unprecedented nature of the ANY plume, with significantly more outlier points, larger maximum mixing ratios, and more rapid ascent than seen in prior events, as well as lofting of the plume into the middle stratosphere. While multiple injection events occurred over several days, back trajectories (not shown) suggest that the pyroCb that produced the P1 plume occurred some time on 30–31 Dec; we use 0 UTC 31-Dec-2020 as the nominal ANY injection time and measure days after ANY (d_{ANY}) referenced to this time. CO reached 400 ppbv at 21.5 hPa by 30 d_{ANY} and exceeded 145 ppbv at 10 hPa by 53 d_{ANY}.

An extended gap in observed CO enhancements 55–60 d_{ANY} (seen at 10 hPa in Figure 1j) results from MLS sampling; the plume lies between successive MLS orbital tracks

and drifts westward at approximately the same rate as the daily MLS longitudinal sampling. That the plume outliers fit neatly into this ∼1100 km gap is an indication of the compactness of the plume, two months after its injection into the stratosphere.

Analogous histograms of MLS H_2O observations are shown in Figures 1n–z. The variability (0–9 ppmv) seen throughout the record in Figure 1n arises almost entirely in the winter polar vortices; positive anomalies result from descent of high values, and negative ones, particularly evident in southern winters, result from condensation of H_2O in polar stratospheric clouds. As above, winter latitudes are excluded from daily histograms (panels 1o–z).

The BS plume (Figures 1o–r) is distinguished from the PNE and ANY plumes by its almost complete lack of elevated H_2O. A small H_2O anomaly at 100 hPa, reaching 8.2 ppmv four days after BS, does not propagate upward even to 82.5 hPa (not shown), and no H_2O abundances as large as 6 ppmv are found to be correlated with high CO anomalies higher in the atmosphere. MLS H_2O has sufficient vertical resolution to be useful in studies of hydrologic processes near the tropopause, but the MLS twice-daily sampling within 24° of longitude at a given latitude is unlikely to, and indeed does not, capture the specific spatially and temporally localized pyroCb stratospheric injections of interest here. Thus, study of dehydration in pyroCbs is beyond the scope of this work, and our attention will be limited to the plumes after horizontal spreading has made them reliably observable by MLS, typically several days after injection.

The PNE was a singular occurrence in the first 15+ years of the MLS stratospheric H_2O record, with 46.4 hPa H_2O mixing ratios as high as 14 ppmv persisting for over 65 days after the event (d_{PNE}) (Figure 1u). At 31.6 hPa (not shown), the plume can be tracked with mixing ratios exceeding 6.5 ppmv until ∼105 d_{PNE} (Pumphrey et al., 2020). Outliers over 80–105 d_{PNE} at 21.5 hPa (Figure 1t) are correlated with the plume, but beyond 100 d_{PNE}, they become increasingly difficult to distinguish from the beginnings of seasonally descending high H_2O anomalies as the plume moves to higher latitudes.

The ANY and PNE plumes have similar maxima at 100 hPa (compare panels 1v and 1z), but the ANY plume has far more outlier observations at all levels (light blue colors in the histogram denote an order of magnitude more occurrences in a bin than dark blue) and ascends more rapidly and much higher into the middle stratosphere than did the PNE plume. H_2O is longer-lived at these levels than CO and gives a better indication of the degree to which the plume remains intact and compact for more than 100 d_{ANY}. Mixing ratios as high as 17.5 ppmv at 10 hPa are seen at 70–80 d_{ANY} (Figure 1w). That anomalies continue to ascend to higher levels is an indication that the particle and the gas-phase components of the thickest parts of the plume remain together, as dense absorptive aerosol is required for sufficient heating to loft the plume (Yu et al., 2019). The gap at 55–60 d_{ANY} seen in 10 hPa CO is also clearly evident in H_2O, further evidence that the plume's trace-gas anomalies are colocated.

Figure 2 shows the 3D time evolution of the ANY H_2O plume location. The primary plume (P1) moves eastward, reaching 120°W by ∼4.5 d_{ANY}, consistent with 100 hPa zonal winds of 18 ms^{-1}. It remains near the southern tip of South America until ∼30 d_{ANY} while ascending to 26.1 hPa, then begins to move steadily westward at ∼9° per day (∼6.5 ms^{-1}), circling the Earth twice while moving slowly northward and ascending to 5.62 hPa by 110 d_{ANY}. During this time, P1 remains just equatorward of a zonal wind reversal to westerlies (multicolored line on Figure 2b); the equatorward motion of this wind reversal after ∼40 d_{ANY} is associated with the formation of the polar vortex (Kuroda & Kodera, 1998, and references therein). Almost all observed mixing ratios >11 ppmv are in P1, but smaller dots corresponding to mixing ratios <9 ppmv show the complex morphology of sub-plumes that are sheared off P1 and caught up in more poleward, westerly flow. The resulting unlabelled sub-plumes have smaller gas-phase abundances than P1, and, as they do not loft appreciably, we infer that they have less opacity from absorptive aerosol. The con-

tinual erosion of P1's southern flank results in the bulk of its constituents eventually moving toward the developing southern polar vortex; incorporation of plume constituents into the vortex could potentially impact winter/spring polar chemical processing. However, significant plume remnants reaching high latitudes (>60°S) after 90 d_{ANY} at 12.1 hPa have much less negative PV than do parcels that fill the already well-developed vortex at this level and are thus unlikely to mix in. Mixing of earlier, lower-altitude sub-plumes into the developing vortex could possibly have occurred before the establishment of a substantial vortex-edge transport barrier, but we see no obvious evidence of that in MLS data.

The heating of absorptive aerosol in P1 not only induces lofting, but also produces a ∼1000-km-diameter anticyclonic vortex, the first reported stratospheric dynamical response to a pyroCb plume (K20; Allen et al., 2020) While meteorological analyses such as MERRA-2 do not model absorptive aerosol and thus have no heating source, nudging of these models to assimilated satellite temperature data is sufficient to drive this response. From 7 to 69 d_{ANY}, the position of the peak of the anticyclone's PV anomaly on Figure 2 clearly tracks the rapidly ascending composition anomalies of P1. The disappearance of this PV anomaly (K20), the slowing of the plume's ascent, and an increase in sub-plumes departing southward and eastward after ∼70 d_{ANY} all indicate that the plume becomes less coherent at this point.

The next largest ANY plume (P2, after K20) is first observable in 100 hPa H_2O on 6.5 d_{ANY}, but does not routinely exceed 7 ppmv until 11 d_{ANY}, when it reaches 80°S, 160°W. P2 remains over the Antarctic Peninsula, at roughly the same longitude as P1, until 35 d_{ANY} (Figure 2), then moves north to 60°S and, on ∼50 d_{ANY} at 21.5 hPa, becomes entrained in westerly flow. P2 has enough absorptive aerosol to loft >7 ppmv of H_2O to 21.5 hPa by 40 d_{ANY} (a level that the PNE arguably reached only on 80 d_{PNE}), but it remains much smaller than P1, which ascends to 14.7 hPa by 40 d_{ANY} and eventually has mixing ratios exceeding 18 ppmv at that level. P2 can be tracked to ∼70 d_{ANY} but never lofts above 21.5 hPa.

P3 and P4 are both eastward-propagating minor plumes that circle the globe in the first 35 d_{ANY}. P3 is not absorptive enough to heat and rise above 100 hPa, but P4, about 10 days behind P3 in its longitudinal progression, rises to 68.1 hPa by 30 d_{ANY}. Two pieces of P3 that were quite close together on 10 d_{ANY} both advect eastward, but by 18 d_{ANY}, the sub-plumes labeled P3 and P3A have diverged by 24° in latitude.

3.2 Multi-constituent ANY Plume Evolution

Figures 3a–f show Southern Hemisphere (SH) histograms of MLS H_2O, CO, and four other biomass burning products for −5 to 120 d_{ANY}. MLS record-high values were observed in the ANY plume on at least some of the levels shown for each of these species.

H_2O (Figure 3a) has record-high values in the ANY plume at all levels from 82.5 to 10 hPa, reaching 21.5 ppmv at 46.4 hPa on 17 d_{ANY}, and with maxima still exceeding 18 ppmv at 10 hPa on 73 d_{ANY}. It has the best combination of vertical (∼3.1 km, slightly coarser than O_3) and horizontal (190–290 km) resolution of any plume constituent measured by MLS and provides a long-lived tracer of plume location to which more poorly resolved species can be compared. Observed H_2O abundances reflect both the plume's strength and the degree to which it fills the MLS field of view. Changes in abundances of plume constituents can be inferred from changes in their correlation with H_2O, but the spatial resolution of H_2O must be degraded to that of a lower-resolution product before comparisons are made (see below and SI). Note, however, that peak values of H_2O at 100–68.1 hPa are slightly lower than those at 46.4 hPa. As the spatial resolution is actually slightly better at 100 hPa than at 68.1 hPa, this deficit in H_2O at 100–68 hPa cannot be explained by blurring of the plume; rather, it may be attributable to some reversible condensation on particle surfaces at the low temperatures present at these levels.

Record-setting values of CO are observed in the ANY plume at all levels 100–21.5 hPa (Figure 3b). The CO measurement resolution does not degrade significantly through the lower stratosphere (Figure S2), so the decrease of CO relative to H_2O is almost certainly attributable to its relatively short lifetime, as discussed further below.

MLS HCN is typically not useful at pressures >21.5 hPa (Livesey et al., 2020), but the record-high values in the ANY plume (Figure 3c) vastly exceed the measurement precision and biases that normally limit its usefulness in the lower stratosphere. Proper interpretation of these data requires consideration of the measurement's spatial resolution, encapsulated in the vertical and horizontal directions by its 2D averaging kernel (**A**) (Livesey et al., 2020, pp. 8–9); summing the responses at each level from all nearby profiles collapses **A** into the more familiar vertical averaging kernels shown in Figure S1. MLS HCN's coarse vertical resolution (∼8–9 km, see Figures S1, S2) makes it appear to extend above the actual plume location (e.g., a record retrieved value at 3.16 hPa, not shown, is a response to HCN at 6.81 hPa) and causes the HCN signal of the rising plume to reach a given pressure surface before better-resolved species like H_2O. Conversely, HCN's arrival at 100 hPa is slighly delayed (compare Figure 3c1 to CO in 3b1) because the HCN retrieval lacks sensitivity at 100 hPa (Figure S1), so the retrieved 100 hPa value does not begin to rise appreciably until the plume reaches 68 hPa. Negative retrieved HCN mixing ratios in panels 3c1 and 3c2 result from negative responses in the HCN 100 and 68.1 hPa averaging kernels at 21.5 and 14.7 hPa (Figure S1).

Despite its relatively long lifetime (over a year in the stratosphere, e.g., Glatthor et al., 2009), HCN appears to decrease in the plume more rapidly than does H_2O; again, this can be explained by its spatial resolution. We can infer a plume HCN/H_2O ratio from regression of anomalies of HCN relative to the zonal mean (ΔHCN) with anomalies of H_2O relative to its zonal mean (ΔH_2O), as shown for 46.4 hPa in Figure 3g. However, if we first blur ΔH_2O to the spatial resolution of HCN, as in Figure 3h, not only is the correlation much tighter (R^2 increases from 0.72 to 0.98), but also the ratio becomes a consistent 3×10^{-4}, when binned either by level (Figure 3m) or by time (Figure S7). When the two products being regressed provide consistently blurred pictures of the plume, their inferred ratio is a better estimate of the true ratios of the species in the plume. Hereinafter, we use H_2O^* to denote H_2O convolved with **A** of the product to which it is being compared, and Δ to denote the anomaly relative to the zonal mean.

MLS CH_3CN (Figure 3d) is generally not considered to be useful at pressures >46.4 hPa (Livesey et al., 2020), but, like HCN, shows record-high values (147–10 hPa) that almost certainly reflect real atmospheric enhancements. The reported stratospheric lifetime of CH_3CN is >70 years (Harrison & Bernath, 2013), and Figure 3m shows the ratio CH_3CN/H_2O to be nearly constant (6×10^{-5}) in the low to middle stratosphere when taken from the regression of ΔCH_3CN with ΔH_2O^*, in contrast to the apparent decay found when regressing against unconvolved ΔH_2O. MLS CH_3Cl (Figure 3e) also has record values (100–14.7 hPa) and an apparent decay (despite its ∼35 year lifetime in the stratosphere, Umezawa et al., 2015) that can be explained by its degrading spatial resolution with decreasing pressure (Figure S2). Figure 3m shows a roughly constant (1×10^{-4}) $\Delta CH_3Cl/\Delta H_2O^*$ ratio. MLS CH_3OH (Figure 3f) spectral signatures are subject to interference from other species, and the retrieval is usually considered marginally useful only at 100–147 hPa, but record-high abundances are observed in the ANY plume from 147 hPa (not shown) to 31.6 hPa (3f1–f4), likely reflecting extraordinarily enhanced atmospheric abundances. Even using ΔH_2O^*, this product clearly decays (shown by a time progression of regressed slopes of ΔCH_3OH with ΔH_2O^* in Figure S7), with an e-folding time of ∼10 days that is consistent with its reported global lifetime (Jacob et al., 2005). Figure S7 also shows the progression in time of slopes from regression of ΔCO with ΔH_2O^*, suggesting a lower/middle stratospheric CO lifetime of ∼30 days, consistent with published estimates for the mid-troposphere (Duncan et al., 2007) and upper stratosphere (Minschwaner et al., 2010).

Figure 3i–l are examples of robust correlations found in the plume between ΔH_2O^* and anomalies of other species for which the plume abundances do not stand out against their global background variability. N_2O is a long-lived tropospheric tracer that maintains a roughly constant ratio with ΔH_2O^* ($\sim 1.5 \times 10^{-2}$, Figures S6, S7).

Tropospheric air in the plume produces a negative perturbation in HNO_3 at 46.4 hPa against its higher stratospheric values. At 10 hPa, background abundances are smaller and HNO_3 is higher inside the plume than outside (Figures S5–S7), suggesting that lower-stratospheric air from near the peak of the background HNO_3 distribution has been incorporated into the plume as it rises, and/or production of HNO_3 has occurred in the plume. To first order, the depression of O_3 in the plume can also be attributed to displacement of ozone-rich stratospheric air by ozone-poor tropospheric air. Yu et al. (2019) found similar negative anomalies in lower stratospheric ozone following the PNE to be consistent with transport of tropospheric air without needing to invoke in situ chemical ozone destruction. The possible influence of chemistry on ozone and HNO_3 abundances in the ANY plume is a topic for further research.

Figures 3h, 3j, and 3l each show an additional, reasonably compact set of correlated points at low values of ΔH_2O^* that do not fall along the black line of the main plume (P1); these points are, in fact, P2. Larger-magnitude negative values of ΔHNO_3 and ΔO_3 are to be expected in P2 since its low values are seen in contrast to the larger 46.4 hPa background abundances at its high-latitude location. That P2 has different correlations of ΔHNO_3 and ΔO_3 with ΔH_2O^* does not necessarily imply that the compositions of P1 and P2 are different. However, the points from P2 in Figure 3h (reaching 0.8 ppbv of ΔHCN at 1.8 ppmv of ΔH_2O^*) have a tight correlation, with a markedly larger slope than that of the bulk of the P1 distribution. Since lower-stratospheric background values of HCN are negligible, this different correlation must be due to different HCN-to-H_2O ratios in P1 and P2. Indeed, as shown in Figure S8, P1, P2, P3, and P4 have different $\Delta HCN/\Delta H_2O^*$ ratios, indicating that they are not fragments of the same plume, but rather that they originate from different pyroCb injections and/or follow different paths into the stratosphere along which they dehydrate differently.

4 Conclusions

Of the three pyroCb events that produced significant, persistent stratospheric plumes in the 16-year MLS record, ANY had by far the largest impact on stratospheric composition, with solar heating of absorptive aerosol lofting record-setting abundances of biomass-burning products H_2O, CO, HCN, CH_3CN, CH_3Cl, and CH_3OH into the middle stratosphere. The largest, densest, most rapidly rising, and most persistent of the plumes produced by the ANY pyroCb complex (P1) rose to 5.62 hPa by 80 d_{ANY}, with H_2O exceeding 7 ppmv until 110 d_{ANY}. P1 became entrained in easterly flow at $\sim$30 d_{ANY} and, over the next 80 days, circled the globe twice at a relatively steady $\sim$6.5 ms^{-1}, gradually moving equatorward to remain just north of the transition to westerlies associated with the developing winter polar vortex. Material sheared off P1's southern side produced multiple sub-plumes that were not dense enough to continue lofting but that moved eastward and poleward toward the developing Antarctic polar vortex. Substantial sub-plumes that split from P1 after 70 d_{ANY} were unlikely to have entered the polar vortex, as the transport barrier in the middle stratosphere was already well-developed by that time. Earlier and lower-altitude sub-plumes may have reached high latitudes before the transport barrier at the vortex edge fully developed, but MLS data give no clear indication that this happened.

Detailed analyses of the ratios of plume constituent abundances using MLS measurements require the degradation of higher-spatial-resolution products (e.g., H_2O) through convolution with the lower-resolution product's averaging kernel, so that the plume in H_2O is spatially blurred in the way that the measurement system blurs the lower-resolution

product. Apparent decay relative to H_2O of species expected to be long-lived in the stratosphere, such as HCN, CH_3Cl, CH_3CN, and N_2O, can be largely explained by the products' coarsening spatial resolution higher in the stratosphere. Regression of long-lived species with appropriately convolved H_2O reveals nearly constant ratios in the plume of $\Delta HCN/\Delta H_2O^*$ ($\sim 3\times10^{-4}$), $\Delta CH_3Cl/\Delta H_2O^*$ ($\sim 1\times10^{-4}$), $\Delta CH_3CN/\Delta H_2O^*$ ($\sim 6\times10^{-5}$), and $\Delta N_2O/\Delta H_2O^*$ ($\sim 1.5\times10^{-2}$). Separate analyses of plumes P2, P3, and P4 in the first 40 d_{ANY} reveals different $\Delta HCN/\Delta H_2O^*$ signatures, a strong indication that these plumes originated from different pyroCb injection events.

Acknowledgments

©2020. California Institute of Technology. Government sponsorship acknowledged. We thank the reviewers for their insightful comments that improved the manuscript. Work at the Jet Propulsion Laboratory, California Institute of Technology, was carried out under a contract with the National Aeronautics and Space Administration. MERRA-2 and MLS data are available from Goddard Earth Sciences (GES) Data and Information Services Center (DISC):

`https://disc.gsfc.nasa.gov/datasets/M2I3NVASM_5.12.4/summary?keywords=Merra-2`
`https://acdisc.gesdisc.eosdis.nasa.gov/data/Aura_MLS_Level2`

`https://acdisc.gesdisc.eosdis.nasa.gov/data/Aura_MLS_Level2/ML2H2O.004/`
`https://acdisc.gesdisc.eosdis.nasa.gov/data/Aura_MLS_Level2/ML2CO.004/`
`https://acdisc.gesdisc.eosdis.nasa.gov/data/Aura_MLS_Level2/ML2O3.004/`
`https://acdisc.gesdisc.eosdis.nasa.gov/data/Aura_MLS_Level2/ML2HCN.004/`
`https://acdisc.gesdisc.eosdis.nasa.gov/data/Aura_MLS_Level2/ML2CH3CN.004/`
`https://acdisc.gesdisc.eosdis.nasa.gov/data/Aura_MLS_Level2/ML2CH3CL.004/`
`https://acdisc.gesdisc.eosdis.nasa.gov/data/Aura_MLS_Level2/ML2CH3OH.004/`
`https://acdisc.gesdisc.eosdis.nasa.gov/data/Aura_MLS_Level2/ML2HNO3.004/`
`https://acdisc.gesdisc.eosdis.nasa.gov/data/Aura_MLS_Level2/ML2N2O.004/`

References

Allen, D. R., Fromm, M. D., Kablick, I., George P., & Nedoluha, G. E. (2020, 10). Smoke With Induced Rotation and Lofting (SWIRL) in the Stratosphere. *Journal of the Atmospheric Sciences*, 1-63. Retrieved from `https://doi.org/10.1175/JAS-D-20-0131.1` doi: 10.1175/JAS-D-20-0131.1

Duncan, B. N., Logan, J. A., Bey, I., Megretskaia, I. A., Yantosca, R. M., Novelli, P. C., ... Rinsland, C. P. (2007). Global budget of CO, 1988–1997: Source estimates and validation with a global model. *Journal of Geophysical Research*, *112*(D22). doi: 10.1029/2007JD008459

Fromm, M., Lindsey, D. T., Servranckx, R., Yue, G., Trickl, T., Sica, R., ... Godin-Beekmann, S. (2010). The untold story of pyrocumulonimbus. *Bulletin of the American Meteorological Society*, *91*(9), 1193–1210. doi: 10.1175/2010BAMS3004.1

Gelaro, R., McCarty, W., Suárez, M. J., Todling, R., Molod, A., Takacs, L., ... Zhao, B. (2017). The modern-era retrospective analysis for research and applications, version 2 (MERRA-2). *Journal of Climate*, *30*(14), 5419–5454. doi: 10.1175/JCLI-D-16-0758.1

Glatthor, N., von Clarmann, T., Stiller, G. P., Funke, B., Koukouli, M. E., Fischer, H., ... Linden, A. (2009). Large-scale upper tropospheric pollution observed by MIPAS HCN and C_2H_6 global distributions. *Atmospheric Chemistry and Physics*, *9*(24), 9619–9634. doi: 10.5194/acp-9-9619-2009

Harrison, J. J., & Bernath, P. F. (2013). ACE-FTS observations of acetonitrile in the lower stratosphere. *Atmospheric Chemistry and Physics*, *13*, 7405–7413.

Jacob, D. J., et al. (2005). Global budget of methanol: Constraints from atmo-

spheric observations. *Geophysical Research Letters*, *110*. doi: 10.1029/2004JD005172

Kablick, G. P., Allen, D. R., Fromm, M. D., & Nedoluha, G. E. (2020). Australian PyroCb smoke generates synoptic-scale stratospheric anticyclones. *Geophysical Research Letters*, *47*(13). doi: 10.1029/2020GL088101

Kuroda, Y., & Kodera, K. (1998). Interannual variability in the troposphere and stratosphere of the southern hemisphere winter. *Journal of Geophysical Research: Atmospheres*, *103*(D12), 13787-13799. Retrieved from `https://agupubs.onlinelibrary.wiley.com/doi/abs/10.1029/98JD01042` doi: 10.1029/98JD01042

Lawrence, Z. D., Perlwitz, J., Butler, A. H., Manney, G. L., Newman, P. A., Lee, S. H., & Nash, E. R. (2020). The remarkably strong arctic stratospheric polar vortex of winter 2020: Links to record-breaking arctic oscillation and ozone loss. *Journal of Geophysical Research: Atmospheres*, *n/a*(n/a). doi: 10.1002/essoar.10503356.1

Livesey, N. J., Read, W. G., Wagner, P. A., Froidevaux, L., Lambert, A., Manney, G. L., ... Lay, R. R. (2020). *EOS MLS version 4.2x level 2 and 3 data quality and description document* (Tech. Rep. No. PL D-33509 Rev. E). JPL. Retrieved from `http://mls.jpl.nasa.gov/` (Available from http://mls.jpl.nasa.gov/)

Manney, G. L., Livesey, N. J., Santee, M. L., Froidevaux, L., Lambert, A., Lawrence, Z. D., ... Fuller, R. A. (2020). Record-low Arctic stratospheric ozone in 2020: MLS observations of chemical processes and comparisons with previous extreme winters. *Geophys. Res. Lett.*, *n/a*(n/a), e2020GL089063. doi: 10.1029/2020GL089063

Minschwaner, K., Manney, G. L., Livesey, N. J., Pumphrey, H. C., Pickett, H. M., Froidevaux, L., ... Boone, C. D. (2010). The photochemistry of carbon monoxide in the stratosphere and mesosphere evaluated from observations by the Microwave Limb Sounder on the Aura satellite. *Journal of Geophysical Research*, *115*. doi: 10.1029/2009JD012654

Peterson, D. A., Campbell, J. R., Hyer, E. J., Fromm, M. D., Kablick, G. P., Cossuth, J. H., & DeLand, M. T. (2018). Wildfire-driven thunderstorms cause a volcano-like stratospheric injection of smoke. *npj Climate and Atmospheric Science*, *1*(1). doi: 10.1029/2020GL088101

Pumphrey, H. C., Santee, M. L., Livesey, N. J., Schwartz, M. J., & Read, W. G. (2011). Microwave limb sounder observations of biomass-burning products from the Australian bush fires of February 2009. *Atmospheric Chemistry and Physics*, *11*(13), 6285–6296. doi: 10.5194/acp-11-6285-2011

Pumphrey, H. C., Schwartz, M. J., Santee, M. L., Kablick, G. P., Livesey, N. J., & Fromm, M. D. (2020). Stratospheric pollution from Canadian forest fires. *Atmospheric Chemistry and Physics Discussions*. (in review) doi: 10.5194/acp-2020-840

Umezawa, T., Baker, A. K., Brenninkmeijer, C. A. M., Zahn, A., Oram, D. E., & Velthoven, P. F. J. (2015). Methyl chloride as a tracer of tropical tropospheric air in the lowermost stratosphere inferred from IAGOS-CARIBIC passenger aircraft measurements. *Journal of Geophysical Research: Atmospheres*, *120*(23). doi: 10.1002/2015JD023729

Waters, J. W., Froidevaux, L., Harwood, R. S., Jarnot, R. F., Pickett, H. M., Read, W. G., ... others (2006). The Earth Observing System Microwave Limb Sounder (EOS MLS) on the Aura satellite. *IEEE Transactions on Geoscience and Remote Sensing*, *44*(5), 1075–1092.

Yu, P., Toon, O. B., Bardeen, C. G., Zhu, Y., Rosenlof, K. H., Portmann, R. W., ... Robock, A. (2019). Black carbon lofts wildfire smoke high into the stratosphere to form a persistent plume. *Science*, *365*(6453), 587–590. doi: 10.1126/science.aax1748

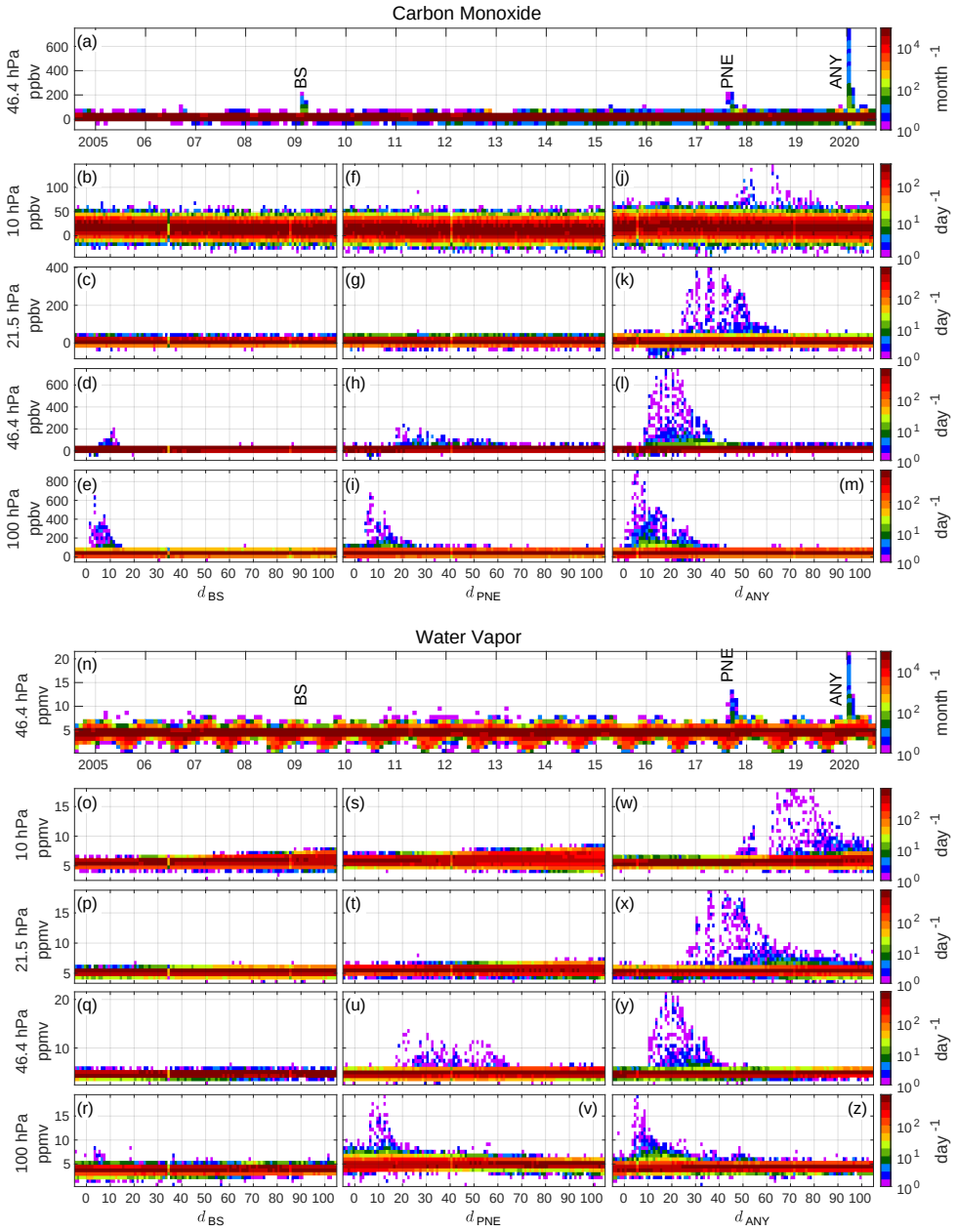

Figure 1. Time series of monthly histograms representing every 46.4 hPa CO (a) and H_2O (n) observation in the MLS record. Outliers are highlighted through use of logarithmic color scales; darkest blue represents a single observation, darkest red represents nearly 10^5 observations. The times of the BS, PNE, and ANY pyroCb events are marked. (b–e), (f–i), and (j–m) Daily histograms of MLS 100, 46.4, 21.5, and 10 hPa CO for 110-day periods after the BS, PNE, and ANY events. (o–z) Analogous daily histograms of H_2O. Daily histograms in (b–m) and (o–z) exclude data from latitudes higher than 20° in the winter hemisphere.

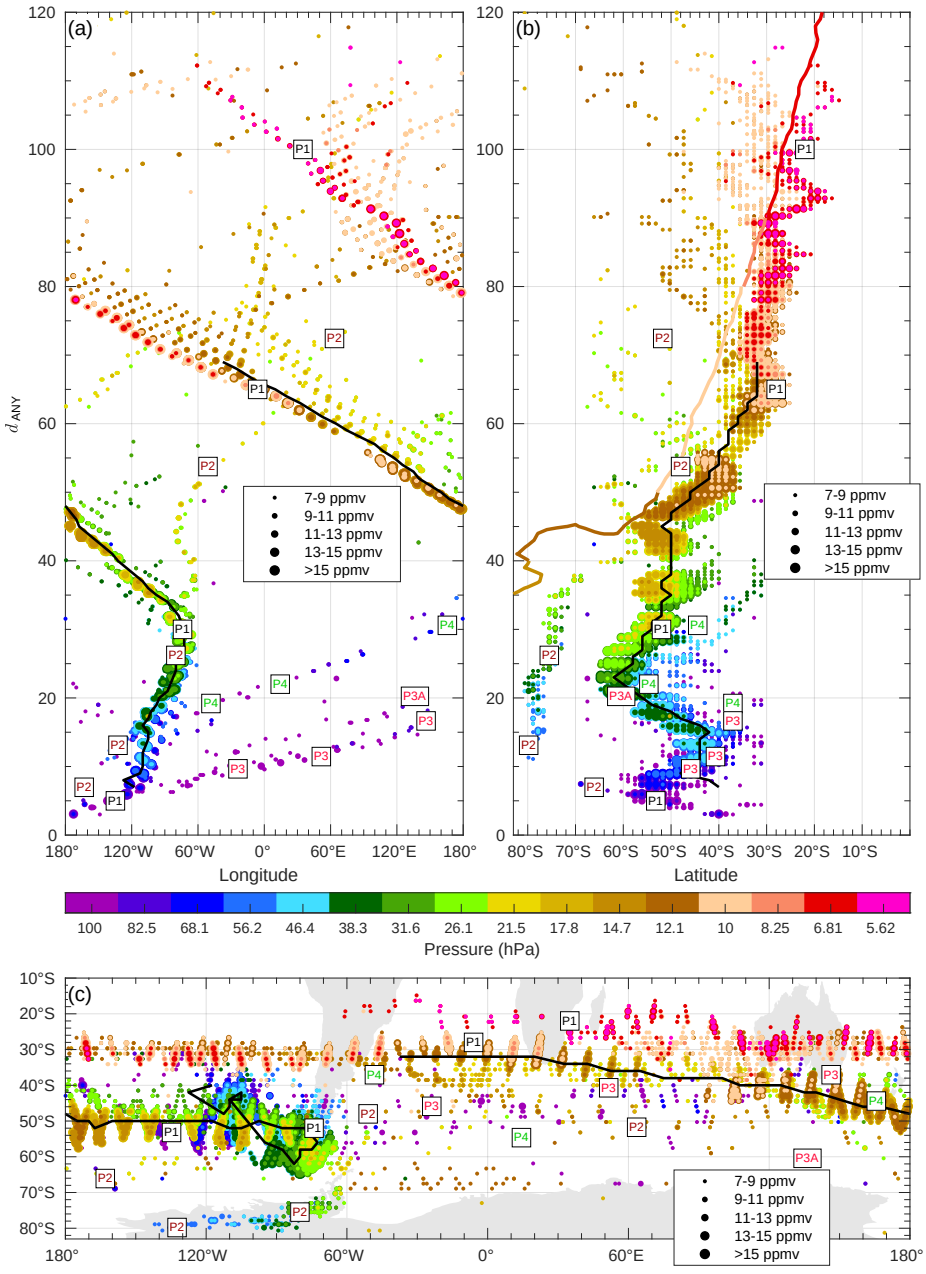

Figure 2. High outliers of H_2O in the 120 days following the ANY pyroCb as d_{ANY} vs. longitude (a) and latitude (b). Data shown exceed time-varying zonal mean values by 1.6 ppmv and also exceed a threshold that varies with dot size (see legend). Dot color denotes the pressure of the MLS retrieval surface exceeding the threshold, with the highest levels (lowest pressures) drawn last and possibly obscuring outliers deeper in the atmosphere. Four plumes, likely originating from different pyroCb injection events, are labeled P1–P4; each plume label appears on all three panels. The zonal-mean zonal wind zero contour at the level of the plume is shown as a multicolored solid line, with the level from which the wind is taken color-coded in the same way as are the outlier points. The black line tracks the daily location of the minimum in the zonal fractional anomaly of MERRA-2 PV absolute value. (c) The same data on a map.

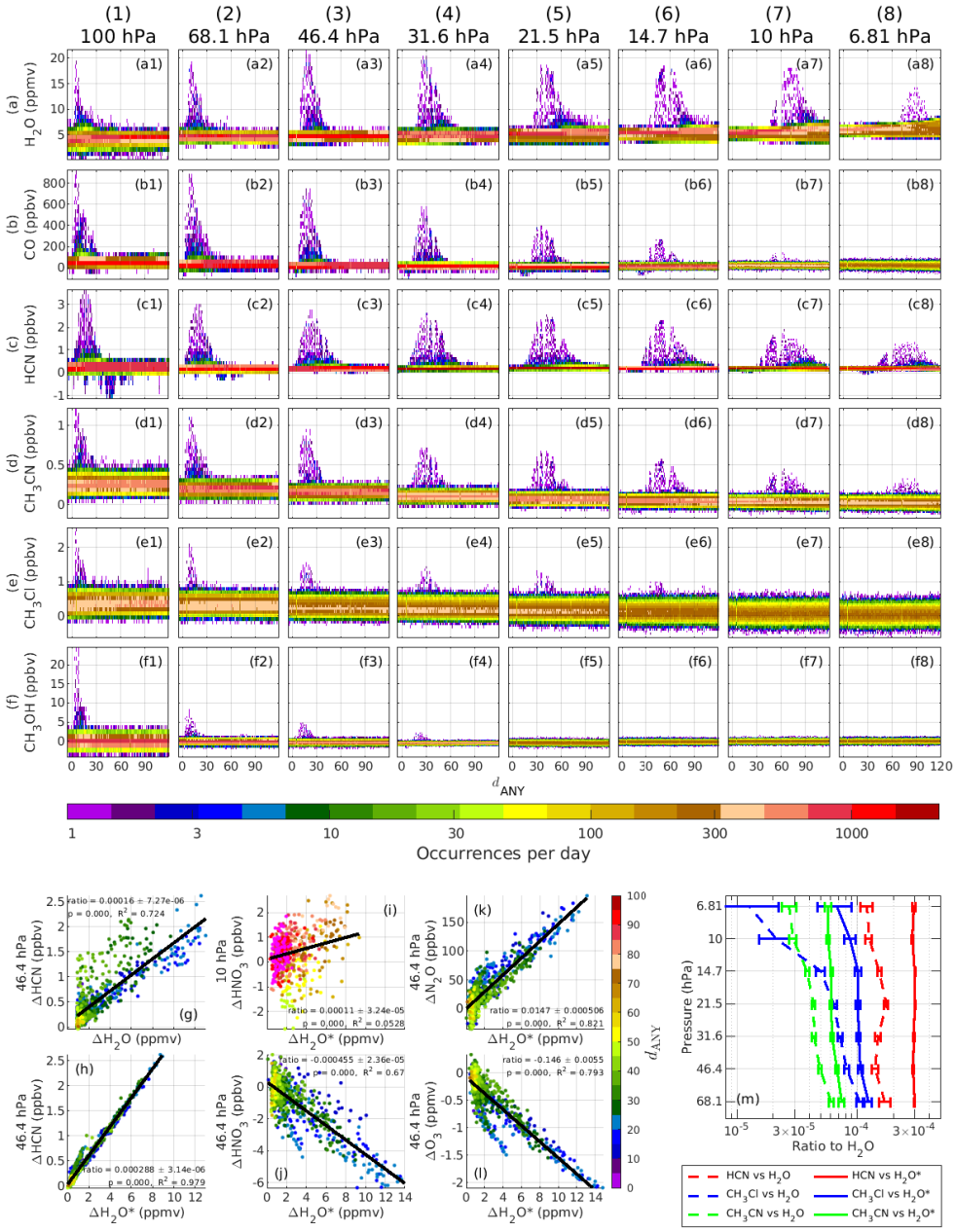

Figure 3. (a–f) Daily histograms for −5 to 120 d_{ANY} of six species with mixing ratio perturbations clearly visible above their background variabilities. (g) Scatter plot of 46.4 hPa HCN departure from its zonal mean (ΔHCN) with respect to H_2O departures greater than 4σ from its zonal mean (ΔH_2O), colored by d_{ANY}. (h) As (g), showing the same profiles, but with ΔH_2O convolved with the averaging kernel (**A**) of the regressed product (ΔH_2O^*). (i–l) As (h), using points with $\Delta H_2O > 4\sigma$ at the given level, but plotted with respect to spatially degraded ΔH_2O^*, for ΔHNO_3 at 10 hPa and ΔHNO_3, ΔN_2O, and ΔO_3 at 46.4 hPa. (m) Profiles of ratios (i.e., slopes of lines on panels g–l) from regression of ΔHCN, ΔCH_3Cl, and ΔCH_3CN with respect to ΔH_2O and ΔH_2O^*, with data restricted to P1, as described in SI.

Figure 1.

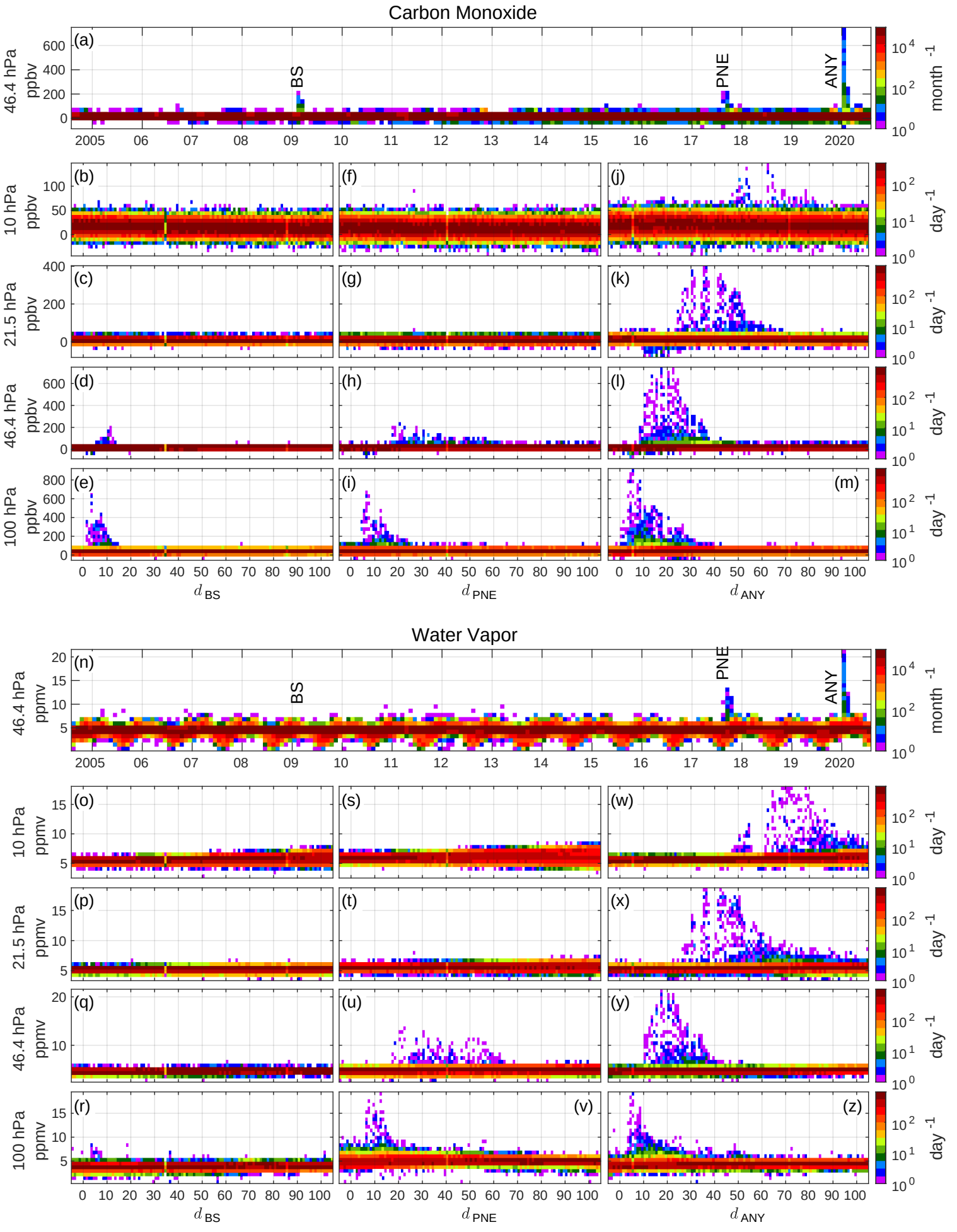

Figure 2.

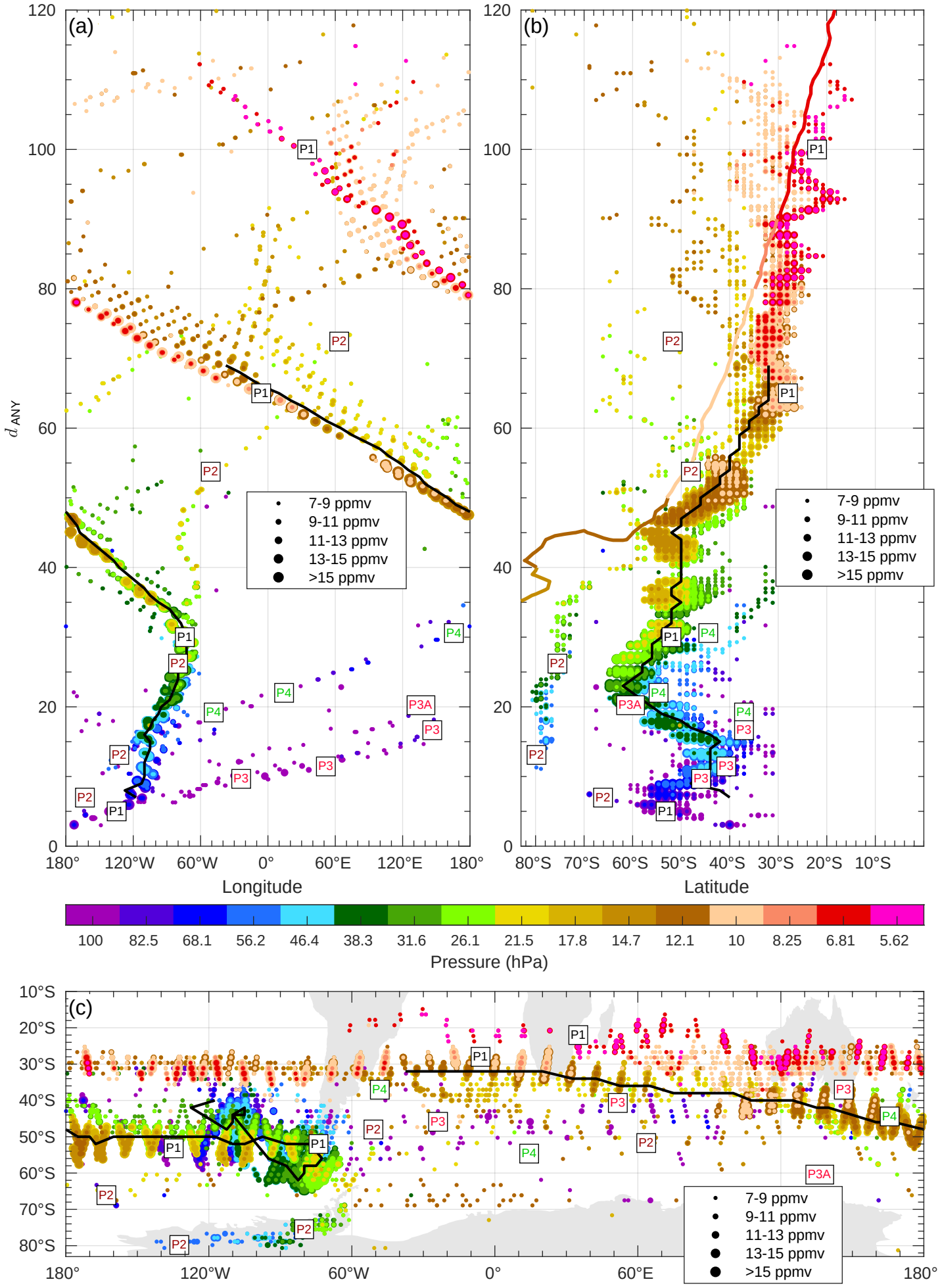

Figure 3.